SYNTHESIS OF TUNGSTEN DISULFIDE (WS_2) AND ITS HYBRIDS BY HYDROTHERMAL METHOD FOR ENHANCEMENT OF PHOTOCATALYSIS

DISSERTATION

SUBMITTED TO
DEPARTMENT OF PHYSICS
SCHOOL OF PHYSICAL SCIENCES
DOON UNIVERSITY, DEHRADUN

IN PARTIAL FULFILLMENT OF THE REQUIREMENTS FOR THE AWARD OF THE DEGREE OF

MASTER
IN
PHYSICS

BY

DEEPALI ASWAL (17PH-18)

DEPARTMENT OF PHYSICS
SCHOOL OF PHYSICAL SCIENCES
DOON UNIVERSITY, DEHRADUN
UTTARAKHAND (INDIA)

2022

SYNTHESIS OF TUNGSTEN DISULFIDE (WS_2) AND ITS HYBRIDS BY HYDROTHERMAL METHOD FOR ENHANCEMENT OF PHOTOCATALYSIS

DISSERTATION

SUBMITTED TO
DEPARTMENT OF PHYSICS
SCHOOL OF PHYSICAL SCIENCES
DOON UNIVERSITY, DEHRADUN

IN PARTIAL FULFILLMENT OF THE REQUIREMENTS FOR THE AWARD OF THE DEGREE OF

MASTER IN PHYSICS

BY

DEEPALI ASWAL (17PH-18)

DEPARTMENT OF PHYSICS
SCHOOL OF PHYSICAL SCIENCES
DOON UNIVERSITY, DEHRADUN
UTTARAKHAND (INDIA)

2022

Declaration

I declare that the work in this dissertation titled **"Synthesis of tungsten disulfide (WS_2) and its hybrids by hydrothermal for enhancement of photocatalysis"** has been carried out byme is submitted to the Department of the physics, School of Physical Sciences,Doon University, Dehradun for the award of Master in Physics is my original research work. The Dissertation embodies the results of investigations, observations, and experiments carried out by me. I have neither plagiarized any part of the dissertation nor have submitted same work for the award of any other degree/diploma anywhere.

……

DEEPALI ASWAL

(17PH-18)

DATE: …../07/2022

Certificate

This is to certify that Dissertation entitled**"Synthesis of tungsten disulfide (WS_2) and its hybrids by hydrothermal, for enhancement of photocatalysis"** submitted by Deepali Aswalhas been done under my supervision. It is also certified that the work in this dissertation embodies original research and hard work of the candidate. The assistance and support received during the course of investigation and all the sources of literature have been fully acknowledged.

Supervisor/Guide
Dr.Himani Sharma
Assistant Professor
Department of Physics
School of Physical Sciences Doon University

Head of Department
Dr.Himani Sharma
HOD in Charge
Department of Physics
School of Physical Sciences Doon University

Acknowledgment

I express my deep gratitude to my project supervisor Dr.Himani Sharma for providing me with the opportunity to work under her supervision and encourage, motivated, supported and provided me such an informative environment during my project work. Her positive criticism and constant assistance and guidance helped me and encouraged me tackling the obstacles and led to develop a positive attitude and appreciation for the subject. I would like to express my deep gratitude to Dr. Priyanka Bamola and research scholar Saurabh Rawat, for their constant support and assistance throughout the project. They worked very hard throughout in introducing us to the lab equipment, apparatuses, machines and their workings. Their constant push and assistance in understanding the concepts and mechanisms had only led to the successful completion of project on time. They developed a good interaction with me along with everybody else and appreciated to ask doubts and helped clearing the doubts regarding any operations of machines and working of required computer applications. They constantly monitored our work and insisted to maintain discipline, cleanliness, and take necessary precaution while operating equipment. Secondly, I would like to express my sincere appreciation to my lab-mates and colleagues Abhinav Bhatt, StutiDhapola, Monika Bisht, Shreya Negi, Bhuvan Singh Bhandari for their cooperation and creating a healthy atmosphere during the course of project. Their collective problem discussing attitude and assistance had been quite helpful.

DeepaliAswal

(17 PH-18)

Abstract

In the recent years there has been considerable interest in the study of Transition metal dichalcogenide layered compounds which is the class of materials composed of transition metal elements and chalcogen atoms (sulfur, selenium or tellurium).

These 2D TMDCs materials show unique electrical, mechanical and optical properties. Thus, the materials can compensate for graphene (metallic material) and hexagonal boron nitride(insulator) for the application of the next generation semiconductor devices.

Tungsten disulfide (WS_2) is a kind of fine chemical product of tungsten.WS_2 was warmly welcomed by oil plant managers because of its better cracking ability, more stable catalytic activity, and longer performance life. Furthermore, WS_2 is an important lubricant with a friction coefficient of 0.01– 0.15.These properties have stimulated many researchers to explore nano-sized WS_2 with different morphologies such as WS_2 nanotubes and WS_2nanorods.The hydrothermal process, as an important elegant method for wet chemistry, has received considerable attention in synthetic nanostructure materials due to the fact that with these process particles with narrow size distribution, little or no micro agglomeration, good crystallization, and phase homogeneity can be obtained. Here, we have prepared successfully WS_2 nanosheets via the hydrothermal process by adding surfactant CTAB. The possible growth mechanism of WS_2 nanostructures has been discussed in detail. Further hybrids MoS_2/WS_2 and TiO_2/WS_2 are prepared for increasing the photocatalytic property. The samples are characterized with Scanning electron microscopy, X-Ray diffraction, FT infrared spectroscopy and UV-vis spectroscopy. WS_2 and its hybrid TiO_2/WS_2 and MoS_2/ WS_2 was further used photocatalytic degradation of methylene blue. A comparative study was conducted to observe the photocatalytic degradation activity (PCA)on methylene blue (MB).

Content

List of Figures

List of Tables

List of Abbreviations

1D - One dimensional

2D - Two-dimensional

3D- three dimensional

TMDCs/TMDs - Transition Metal Dichalcogenides

WS_2- Tungsten disulfide

MoS_2 - Molybdenum Disulfide

TiO_2- Titanium dioxide

S – Sulfur

W- Tungsten

Mo – Molybdenum

Ti- Titanium

XRD - X-Ray Diffraction

SEM - Scanning Electron Microscope

λ – Wavelength

Θ - Angle of incidence

BSE - Back Scattered Electron

SE - Secondary Electrons

DI - De-Ionized

IPA- isopropyl

eV- electron volt

MB- methylene blue

PCA- photocatalytic activity

g-Gram

cm- centimeter

DI- Dionized water

FTIR- Fourier transform infrared spectroscopy

UV-Vis- Ultra violet visible

ml –Millilitre

mol/L- mole per liter

CTAB- Cetrimonium bromide

h- Planck constant

E_g –band gap

α- alpha

η –neta

Xe- Xenon

Chapter 1

Introduction

1.1 Background

In the recent years, there has been considerable interest in the study of transition metal dichalcogenides(TMDC/TMD) layered compound, which are the class of material composed of transition metal elements and chalcogen elements(sulfur, selenium or tellurium).

TMDs are 2D semiconductor materials showing unique electrical, mechanical and optical properties. Thus, the materials can compensate for graphene (metallic material) and hexagonal boron nitride (insulator) for the application of the next generation semiconductor devices[1], [2].

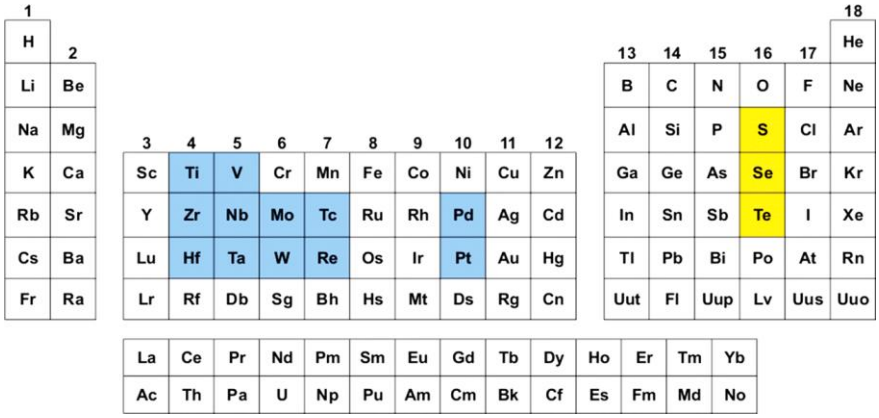

Fig: 1.1The transition metals in blue and the three chalcogen elements in yellow.
(SOURCE: Functionalization of 2D transition metal dichalcogenides for biomedical)

TMDC monolayer's are automatically thin semiconductor of the type MX_2,

Were, **M= Transition metal (Mo, W etc.)** and **X=One of the three Chalcogen atom(S, Se or Te)**

Here one layer of M is sandwiched between two layers of X atoms. They are the part of the large family of 2D materials.TMD monolayers MoS_2 ,WS_2,$MoSe_2$,WSe_2 etc have a direct band gap, and can be used in electronicsas

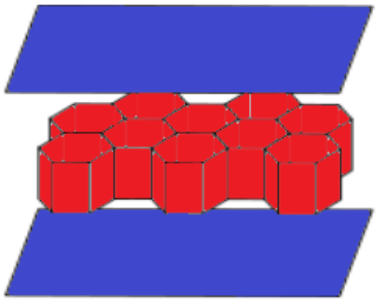

Figure: 1.2 Sandwiched layer

transistors and in optics as emitters and detectors.These are the group of anisotropic materials with strong bonding within the layers and weak interlayer interactions.

1.2 Tungsten Disulfide

As one of the members of this family, WS_2 has attractedconsiderable attention, due to its extensive applications ascatalysts, lubricants, lithium battery, and so on.As we allknow, properties of the matter are limited by it size, shapeand specific surface area. Compared with WS_2 bulkmaterials, microscale or nanoscale WS_2 materials havemore favourable properties such as larger specific surfacearea, etc. The interest in exploration of generating nanoscaleWS_2 with specific morphologies and unique properties by using different approaches keeps increasing.Tungsten disulfide (WS_2) is a kind of fine chemical product of tungsten.WS_2 was warmly welcomed by oil plant managers because of its better cracking ability, more stable catalytic activity, and longer performance life. Furthermore, WS_2 is an important lubricant with a friction coefficient of 0.01– 0.15. These properties have stimulated many researchers to explore nano-sized WS_2 with different morphologies such as WS_2 nanotubes and WS_2 nanorods[3]–[5]Among different monolayer TMDCs, tungsten disulfide fascinates due to its electronic band gap which undergoes an indirect (1.4eV) to direct (2eV) transition when its size is reduced from bulk to monolayer. In monolayer form, WS_2 nanosheets have numerous applications including photocatalysis which is the main application of this particular thesis[6], [7].

1.2.1 Crystal structure

Like other TMDCs family member Tungsten Disulfide have a 2D structure. It occurs naturally as the rare mineral tungstenite. It consists of a layer of hexagonally-arranges tungsten atoms[3], |

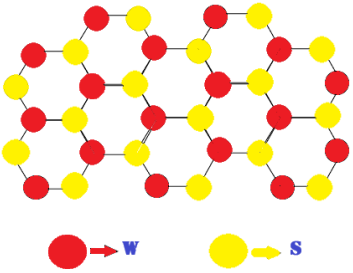

Figure 1.3 Crystal Structure of WS_2

positioned between two layers of hexagonally arranged Sulphuratoms.Tungsten disulfide (WS_2) has a graphite-like structure with the properties of strippable and indirect/direct band gap conversion. Individual layers are held together by Van der Waals forces. This makes it possible for single to few layerultra-thin films to be prepared from bulk crystals using mechanical exfoliation techniques.The primitive unit cell of WS_2 consist of one tungsten atom and two sulphur atoms, arranged in a trigonal prismatic configuration.

1.2.2 Physical properties

Tungsten disulfide is dry(solid lubricant) powder and is one of the most lubricious substances in world. WS_2 offers excellent dry lubricity unmatched to any other substance, including graphite or molybdenum disulfide(COF:0.03)[8], [9].it can also be used in high temperature and high-pressure applicat

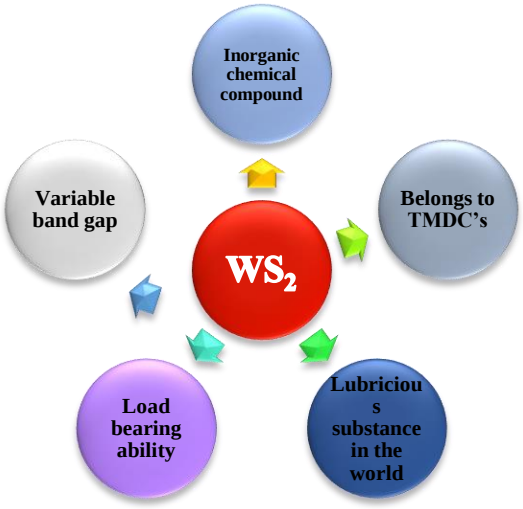

Figure1.4: Physical properties of WS_2

WS_2 offers temperature resistance from -450^oF to 1200^oF(-270^oC to 650^oC)in normal atmosphere and from -305^oF to 2400^oF(-188^oC to 1316^oC) in vacuum. Load bearing ability of coated film is extremely high. Tungsten disulfide nanoparticles are partially soluble in water and acidic solutions.

Table1. 1 Properties of Tungsten disulfide

Chemical formula	WS_2
Group	Tungsten-6 Sulfur -16
Electronic configuration	Tungsten [Xe] $4f^{14}$ $5d^4$ $6s^2$,Sulfur [Ne]$3s^2$ $3p^4$
Molar Mass	247.98g/mol
Density	7.5g/cm^3
Melting point	125^{o}0C
Colour	Silver- grey
Magnetism	Non-magnetic
Chemical durability	Inert substance non toxic

1.3 Molybdenum Disulfide

It is an inorganic compound composed of molybdenum and sulfide atoms. Its chemical formula is MoS_2**.** The compound is classified as a transition metal dichalcogenides. It is a silvery black solid that occurs as the mineral molybdenite, the principal ore for molybdenum. MoS_2 is relatively unreactive. It is unaffected by dilute acids and oxygen. In appearance and feel, molybdenum disulfide is similar to graphite[10]–[12]. It is widely used as a dry lubricant because of its low friction , indirect bandgap semiconductor similar to silicon, with a bandgap of 1.23 eV.

1.3.1 Crystal structure and physical properties:

MoS_2 also have a 2D structure. All forms of MoS_2 have a layered structure, in which a plane of molybdenum atoms is sandwiched by planes of sulfideions. Bulk MoS_2 consists of stackedmonolayer's, which are held together by weak VanderWaals Interactions[13]–[15].

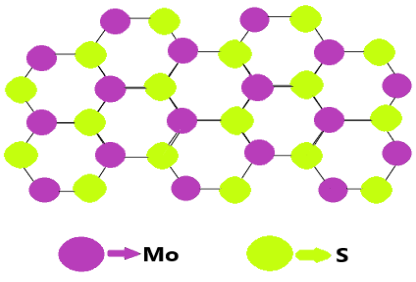

Figure1.5 Crystal structure of MoS_2

Table1. 2 Properties of Molybdenum disulfide

Chemical formula	MoS_2
Group	Molybdenum-6 Sulphur-16
Electronic configuration	Molybdenum[Kr] $4d_5$ $5s_1$Sulphur [Ne]$3s^2$ $3p^4$
Molar Mass	160.07g/mol
Density	5.06 g/cm^3
Melting point	$2,375^0$C ($4,307^0$F)
Colour	Lead grey solid-black
Magnetism	Non-magnetic
Chemical durability	Inert substance non toxic

1.4 Titanium Dioxide

Titanium dioxide is a white inorganic compound. it is dependent on it for its non-toxic, non-reactive and luminous property, which highly whiteness and brightness many materials. It is naturally occurring mineral that is mined from the earth, processed and refined and added to a variety of foods as well as other consumer products[16]–[18]. In natural state it exists in different bulk crystalline forms, such as anatase and rutile but during processing it is ground into a very fine powder. As a photocatalyst it can improve the efficiency of electrolytically splitting water into hydrogen and oxygen and it can produce electricity in nanoparticles form.

1.4.1 Crystal structure and physical properties:

In all three of its main dioxides, titanium exhibits octahedral geometry, being bonded to six oxide anions. The oxides in turns are bonded to three Ti centres. The overall crystal structure of rutile is tetragonal in symmetry whereas anatase and brookite are orthorhombic. The oxygen substructures

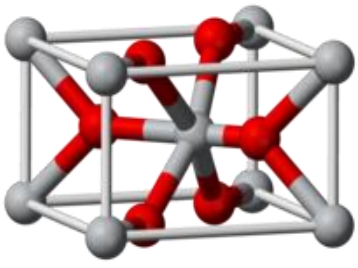

Figure: 1.6 Crystal structure of TiO_2

are all slight distortions of close packing: in rutile, the oxide anions are arranged in distorted hexagonal close-packing, whereas they are close to cubic close-packing in anatase and to "double hexagonal close-packing" for brookite[19], [20]. The rutile structure is widespread for other metal dioxides and difluorides.

Table1. 3 Properties of Titanium dioxide

Chemical formula	TiO_2
Electronic configuration	[Ar] $3d^2$ $4s^2$[He] $2s^2$ $2p^4$
Molar Mass	79.866 g/mol
Density	4.23 g/cm^3
Melting point	1,843 °C
Colour	White solid
Magnetic susceptibility	$+5.9 \cdot 10^{-6}$ cm^3/mol

1.5 Photocatalysis

Disinfection of bacteria is of particular importance, because traditional methods such as chlorination are chemical intensive and have many associated disadvantages. For example, in water treatment applications, chlorine used for disinfection can react with organic material to generate chloro-organic compounds that are highly carcinogenic. Extensive research in this field has been done in the area of photocatalytic removal of organic, inorganic, and microbial pollutants.Due to widespread industrialization an increase in the level of contaminants in the water bodies such as organic pollutants, dyes and other toxic chemicals have been reported.These chemical discharges (Figure 1.7) accumulate in water bodies and cause serve harm to ecosystem as well as living being.

Figure 1.7 Chemical discharges in water bodies

Reported by a global survey portable water will be reduced to 15% in the next 15 years. The problem of water pollution exists worldwide and there is dire need to remove the pollutants from water bodies. Various non-biodegradable and toxic pollutants generated as a chemical waste from agrochemical, paper and pharmaceutical industries are dumped in water bodies[8], [19].

One such toxic dye, Methylene blues (MB) figure 1.7, a cationic dye is widely used in paper and textile industries; however, it has many drawbacks to its usage.

Figure1.8 Methylene blue dye

Not only this dye cause water pollution but also when consumed by living beings can be a major cause of increase heart rate, jaundice etc.Side effects of large doses of Methylene Blue include chest pain.

1.5.1 Why photocatalysis

It has been reported that photocatalysis is an effective method for the removal of wide spread of pollutants. It uses solar energy as a source to form radicals that oxidize these pollutants and cause their catalytic degradation.

In present case scenario a lot of research has been conducted on the photocatalytic activity of various nanostructures. Manynanocomposite photocatalytic have been developed to enhance the visible –light driven photocatalytic activity with reduced electron hole recombination, yet it remains a challenge to attain very high efficiency with less complexity.

1.6 Semiconductors as photocatalystand mechanism of photocatalysis

Photocatalyst is a material that functions as catalyst when exposed to light and the photocatalytic activity (PCA) depend on the ability of catalyst to create electron hole pairs, which generate free radicals when holes interact with the dye[2], [8], [18], [19], [21].

Common heterogeneous photocatalyst are TMDC and semiconductorsas they possess forbidden energy band gap which needs visible light to promote electron from valance band to conduction band. This forms positive hole in valance band and free electron in conduction band i.e., electron-hole pair formation takes place.

In the photocatalytic process a semiconductor is commonly used, which is non-toxic, chemically stable, available at reasonable cost, and capable of repeated use without substantial loss of catalytic ability Up to now heterogeneous semiconductor materials like ZnO, Fe_2O_3, CdS, ZnS, TiO_2, SnO_2, WO_3, $LiNbO_3$ are used as photocatalyst. [18], [19]

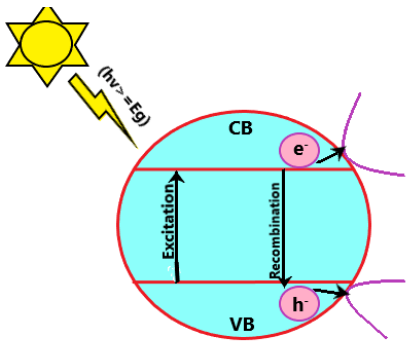

Figure: 1.9 Semiconductor as photocatalysis.

The photocatalysis is a versatile and efficient disinfection process capable of inactivating a wide range of harmful microorganisms. This method has a number of advantages, such as requiring a simple reactor, no secondary pollution left by the degraded organic substances, and able to be reprocessed in an eco-friendly approach.Due to generation of positive holes and free electron, oxidation and reduction reactions takes place at the surface of the semiconductor.

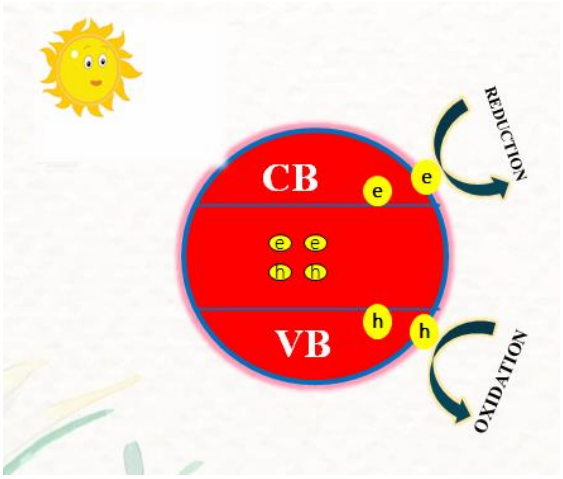

Figure 1.10 Mechanism of photocatalysis

In oxidation reaction the positive holes react with the moisture present on the surface and produce hydroxyl radicals as shown in figure 1.10. Due to the reactions of electron and hole there is generation of free radical and this hydroxyl radical is one of the strong oxidizing agents and plays an important role in application of photocatalysis during photodegradation of dyes, pesticides etc.

- Holes + reductant =oxidized product
- Excited electron +oxidant = reduced product

1.6.1Types of photocatalysis

There are two type of photocatalysis (figure 1.11).For instance, the photo-assisted degradation of aqueous organic dye using water soluble carbon dots is homogeneous photocatalysis. On the other hand, if the photocatalyst and the reaction medium are not in the same phase, then it is called as heterogeneous photocatalysis.

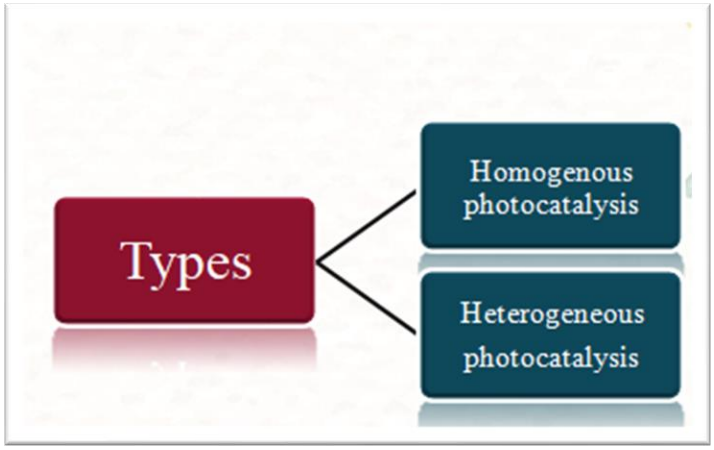

Figure1.11 Types of photocatalysis.

Homogenous Photocatalysis-here both reactant and photocatalyst exists in the same phase.

Heterogeneous Photocatalysis- here the catalysis is in different phase from the reactant.

Chapter 2

Synthesis and Characterization Techniques

2.1 Introduction

In this chapter various synthesis techniques and characterization techniques with their working mechanism are discussed in details.The mechanism of synthesis techniques namely anodization and hydrothermal process are elaborated, moreover the instrumentation of these techniques is briefly discussed.The chapter objective is to also summarize the present knowledge on the use, advantages and weaknesses of a large number of experimental techniques that are available for the characterization of nanoparticles.

2.2 Synthesis techniques

Nanoparticles synthesis refers to methods for creating nanoparticles. The different methods which are being used to synthesize nanomaterials are chemical vapour deposition method, thermal decomposition, hydrothermal synthesis, solvothermal method, pulsed laser ablation, templating method, combustion method, microwave synthesis, gas phase method, and conventional Sol-Gel method.

2.3Approaches for the synthesis of nanomaterials

Several methods have been developed to produce metal nanoparticles.Two main approaches are used for the synthesis of nanomaterials: top-down approaches and bottom-up approaches shown in figure2.1.

Each approach is quite simple—the top-down approach goes from the general to the specific, and the bottom-up approach begins at the specific and moves to the general.

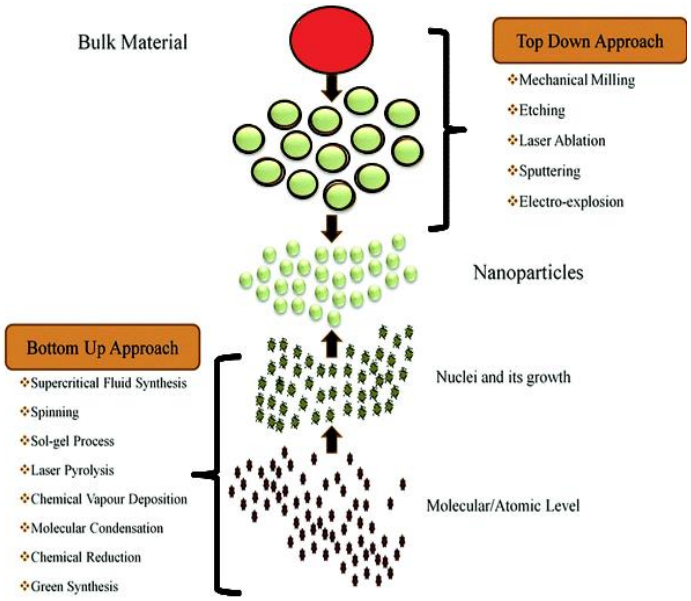

Figure 2.1The synthesis of nanomaterials via top-down and bottom-up approaches.

2.3.1 Top DownApproaches: In top-down approaches, bulk materials are divided to produce nanostructured materials. Top-down methods include mechanical milling, laser ablation, etching, sputtering, and electro-explosion. Top down involves the mechanical method to crush/breaking the bulk to several parts to form nanoparticles as shown in fig 2.2(b).

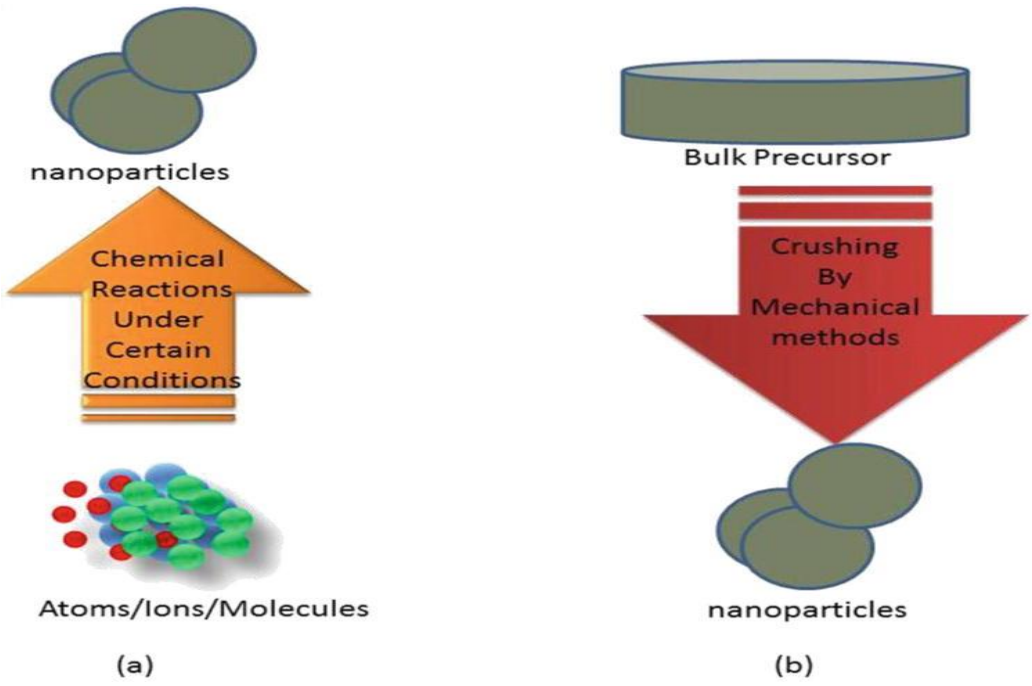

Figure 2.2 Synthesis approaches for nanoparticles (a) bottom up and (b) top down approaches.

2.3.2 Bottom-up Approach: The alternative approach, which has the potential of creating less waste and hence the more economical, is the 'bottom- up'. Bottom-up approach refers to the build-up of a material from the bottom: atom-by-atom, molecule-by-molecule, or cluster-by cluster shown Fig 2.2(a). Many of these techniques are still under development or are just beginning to be used for commercial production of nano powders. Organometallicchemical route, revere-micelle route, sol-gel synthesis, colloidal precipitation, hydrothermal synthesis, template assisted sol-gel, electrodeposition etc, are some of the well-known bottom–up techniques reported for the preparation of luminescent nanoparticles.

2.4Anodization (two electrode system)

Anodization is an electrolytic process used to increase the thickness of natural oxides layers on the surface of the metal part.The process is a called anodization because the part to be treated from the anode electrode of an electrolytic cell shown in figure 2.3. Anodization changes the microscopic texture of the surface and the crystal structure of the metal near the surface.

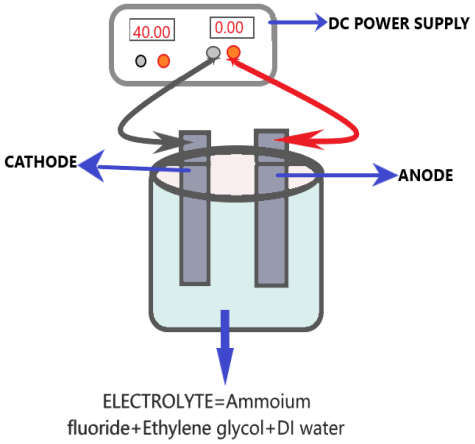

Figure 2.3Electrochemical anodization set up

2.4.1Mechanism of anodization:

The anodization begins and the current passes through the electrolyte. This current leads to the formation of ions in the electrolyte henceforth resulting in the movement of ions towards oppositely charged electrodes. Oxidation (i.e., the discharge of negative charged ions) at

anode takes place whereas reduction (i.e., gain of electron) at the cathode of the electrochemical cell takes place. Later the current decreases as the formation of high resistive compact oxide layer on the surface of anode as the process continues small pits are formed on the surface of the compact layer followed by the formation of nanoporousstructures. At the final stage the current density attains a constant value owing to the formation of nanotubes[22], [23]. The formation of nanotube layers on anode can occur under well-defined voltage conditions and long processing periods and electrolytes containing high negative (-ve) ions content.Anodising is an electrochemical process that converts a metal surface into a decorative, anodic oxide finish[21].

2.5 Hydrothermal process

Hydrothermal process is defined performing chemical reaction in solvent contained in a sealed vessel in which the temperature of the solvent can be brought near the critical temperature via heating concurrent with autogenous pressure.The process being called hydrothermal process because the process uses water as the solvent. Hydrothermal synthesis refers to the heterostructure reaction for the synthesis of inorganic materials in aqueous media above ambident temperature and pressure.

Figure 2.4 Hydrothermal Oven

Hence hydrothermal method is a chemical reaction in water, in sealed pressure vessel which is reaction in both high temperature and high pressure.The process an aqueous mixture of precursors is heated in a seated stainless-steel autoclave above the boiling point of water and consequently the vapors pressure within the reaction autoclave is dramatically inversed above the atmospheric pressure.

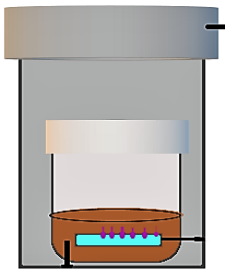

Figure 2.5 An Autoclave

The autoclave (figure 2.5) is a stainless-steel hollow container able towithstand high pressure and temperature. A teflon vesselsinserted in the hollow autoclave, later this vessel is filled with appropriate electrolyte[24], [25]. The autoclave is later sealed tightly and put inside a hot air oven (figure 2.4) for further hydrothermal reaction or process.

2.5.1 Mechanism of hydrothermal reaction

The synthesis of hydrothermal method has usually two steps shown in figure 2.5

- **CRYSTAL NUCLEATION** occurs when the solubility of the solvent is exceeded and no more solvent can be dissolved. The solute precipitates into clusters of crystals that can be grown to microscopic size.

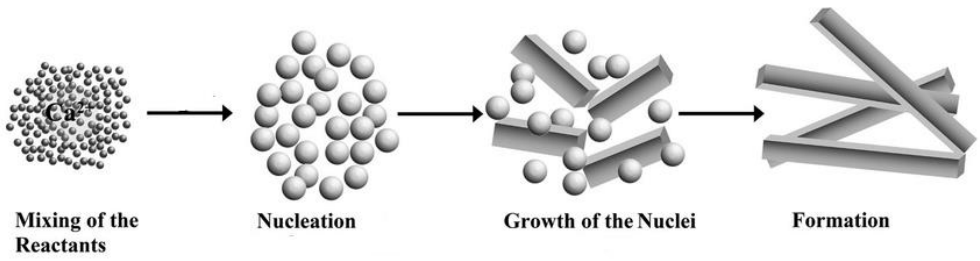

Figure 2.6Diagrammatic sketch of hydrothermal synthesis mechanism

- **SUBSEQUENT GROWTH** the crystal grows subsequently via series of processes involving the incorporation of the growth units which not only have the same composition in the crystal entities but also possess the same or different structures from the bulk solution.

2.6 Characterization Techniques

Several techniques have been used to characterize the size, crystal structure, elemental composition and a variety of other physical properties of nanoparticles. In several cases, there are physical properties that can be evaluated by more than one technique. There are two forms of characterization techniques which are shown in below table. Furthermore, the construction and mechanics of characterization techniques namely X-RAY DIFFRACTION, RAMAN SPECTROSCOPY, SCANNING ELECTRON MICROSCOPY, FT INFRARED AND UV SPECTROSCOPY are briefly discussed in this section.

2.7X-Ray diffraction (XRD)

XRD Characterization is a powerful nondestructive technique for characterizingcrystalline material. It is used to identify the crystalline phase present in a material and thereby reveal chemical composition information.XRD is one of the most widely used techniques for the characterization of nanoparticles.

XRD provides information regarding, crystalline structure, nature of the phase, lattice parameters and crystalline grain size.

2.7.1 Minimum and basic condition - An electromagnetic radiation can be diffracted by atomic planes only when half of its wavelength is less than the interatomic distance d, i.e.

$$\lambda/2 \leq d$$

XRD is based on constructive interference of monochromatic x-rays and a crystalline sample.

Bragg's law **is** a simplistic model to understand what condition are required for diffraction (figure2.7)

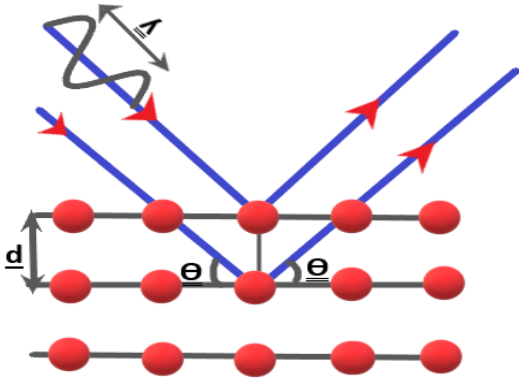

Figure 2.7 Braggs law

The path difference between ray1 and ray2 =2dsinΘ.

For constructive interference: - $\mathbf{2dsin\Theta = n\lambda}$ **(1)**

Where, λ=wavelength of X-Ray

Θ=angle between the incident rays and the surface of crystal

d=spacing between layers of atoms

n=integer (whole number)

Information from Bragg's law for XRD: -

The Braggs law provides us information regarding space between diffracting planes of atoms determines peak position andthe peak intensity is determined by what atoms are in the diffraction planes.

X-Ray diffraction is based on the scattering of x-ray by crystal. Every crystalline substance always gives a pattern, the same substance always gives the same pattern and in a mixture of substance each produces its pattern independently[26].

"So, x-ray diffraction pattern of a pure substance is called the finger print of the substance".

The pattern is the plot of intensity of x-rays scattered at different angles by the sample. The composition of the particles can be determined by comparing the position and intensity of the

peaks with the reference patterns available from the JOINT COMMITTEE ON POWDER DIFFRACTION STANDARDS (JCPDS) database.

2.7.2 X-Ray Diffractometer

A Diffractometer (figure 2.8) is a measuring instrument for analyzing the structure of a material from the scattering pattern produced when a beam of radiation or particles (such as X-rays) interacts with it. X-Rays are generated by a cathode ray tube, filtered to produce monochromatic radiation, collimatedto concentrate and directed towards the sample. The interaction of incident rays with the sample produces constructive interference when conditions satisfy Bragg's law.

- The detector moves in a circle around the sample.
- The detector position is recorded as the angle 2Ɵ.
- The detector records the number of X-Ray observed at each angle 2Ɵ.
- The x-ray intensity is usually recorded as "counts" or as counts per second
- To keep the X-Ray beam properly focused the sample also rotates.

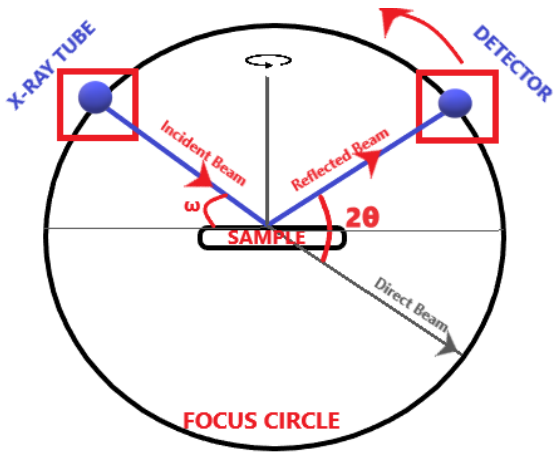

Figure 2.8 X-Ray Diffractometer

2.8Scanning electron microscopy (SEM)

Scanning Electron Microscopy (SEM) gives information about the surface topology and composition of the sample. SEM gives the image formed by scanning the sample surface by

focussed electron beam. Due to very narrow electron beam SEM microgram have a large depth of field, yielding to characteristic 3D image of the surface structure of the sample.

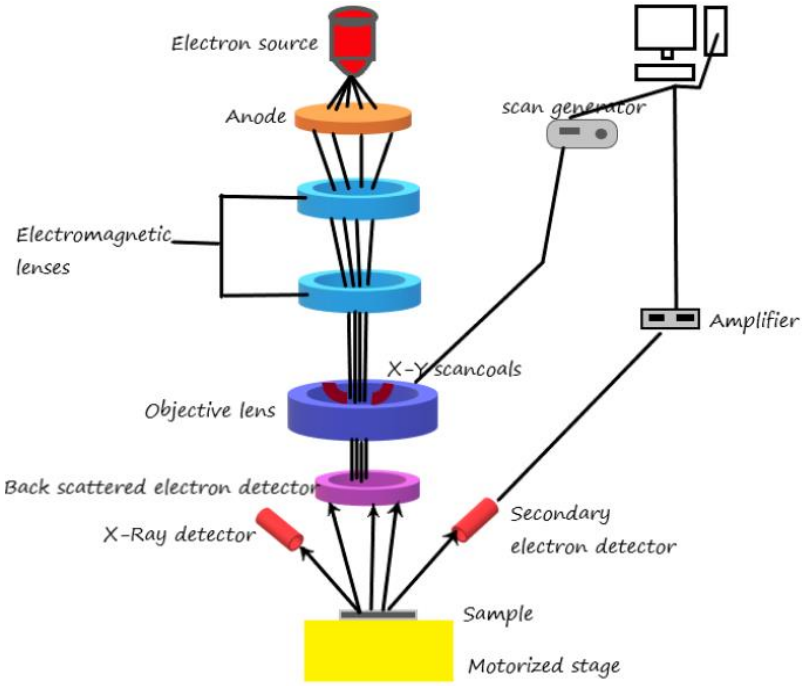

Figure 2.9 Schematic of scanning electron microscope

2.8.1 Mechanism of SEM

In SEM (figure 2.9), thermionic cathode (tungsten) acts as the electron gun inside the microscope producing the primary electrons. The beam of these electrons is produced by the help of anode, which later is focussed by an electromagnetic lens on the substrate. The highly focussed electron beam can be deflected to different parts of the substrate with the help of electromagnetic deflector. When a beam of highly focussed electron is made incident on a sample various types of signals are produced including secondary electrons (SE), Back Scattered Electron (BSE), characteristic X-ray and light (cathode luminescence)[2], [15].

Scanning electron microscopy is based on the detection of secondary electrons. Secondary electrons are produced when electron beam ejects an electron form the atom of the sample. Secondary Electron have a very low energy ~50ev which limits the mean free path in solid

matter. Thus, secondary electrons can escape from top few nano-meters of the sample surface. These secondary electrons are detected by the SEDetector inside the specimen chamber of the microscope. The signal from secondary electrons is localised at the point of impact of primary electron beam, making it possible to collect images of sample surface with resolution of 1nm. The energy exchange between the electron beam and the sample results in the reflection of high-energy electrons by elastic scattering, emission of secondary electrons by inelastic scattering and the emission of electromagnetic radiation, each of which can be detected by specialized detectors. The secondary electrons of the specimen are detected and used to create images of the distribution of specimen current.

2.9 Raman spectroscopy

Raman spectroscopy is a molecular spectroscopic technique that utilizes the interaction of light with matter to not only yield information about the intra and inter molecular vibrations but also gives us additional information about the lower frequency modes and vibrations. That gives insight of crystal lattice and molecular backbone construction.

2.9.1 Mechanism

The change in the wavelength of the incident laser to the scattered wavelength from vibrational bonds between the atoms reveals the contents of the sample. The Raman spectroscopy looks at the change in the molecular bond polarizability. As a photon is incident on a molecule it can induces deformation in the electron cloud. Molecular bonds have specific energy transition in which a change of polarizability occurs, giving rise to Raman active modes.

When light is incident on a molecule, the vast variety of photons are scattered at the same energy as the incident photon, called elastic scattering or Rayleigh scattering. Very small amount of photon will scatter at different frequency, inelastic scattering resulting in the

molecule advancing to a higher energy state and molecule reaching a vibrational level different from that of the beginning state producing a photon of different energy

1: If the change in energy of the scattered photon is less than the incident laser photon it is called strokes scattering

2: If the change in energy of the scattered photon is more than the incident laser photon it is called anti-strokes scattering.

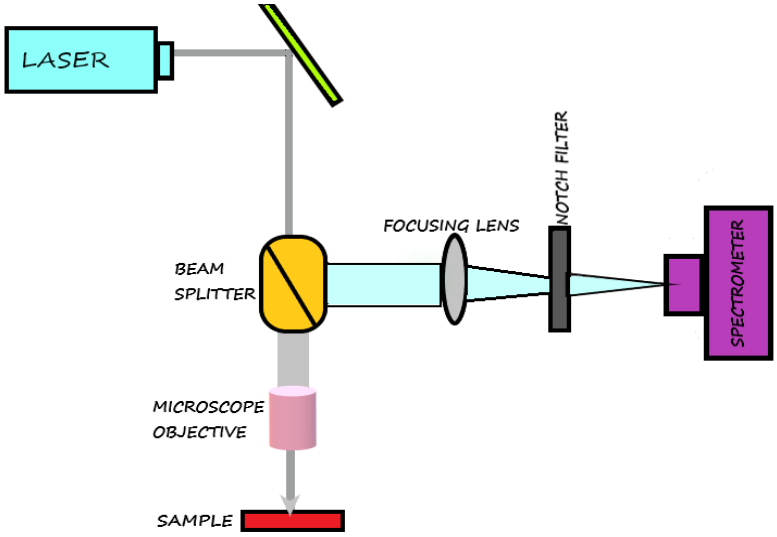

Figure 2.10 Schematic of Raman spectroscopy

This emitted energy passes through a spectrograph which divides it into a spectrum of light. A CCD (charged coupled device) detector analyses the spectrum and turns it into a readout on the Intensityvs. Raman shift graph. The peaks in the Raman spectra represent the different vibrational modes of the crystal molecular bonds.

Each molecular compound having its own unique spectral finger print composed of these vibrational modes, help detection of the sample.

2.10 FTIR (Fourier Transform Infrared Spectroscopy)

FTIR (Fourier Transform Infrared Spectroscopy) is a technique used for obtaining the emission, absorption and photoconductivity of a sample. The sample can be all solid, liquid and gas.

The FTIR (Fourier Transform Infrared Spectroscopy) is a technique which uses infrared radiation for detection of functional group or types of functional group in the sample. The spectrum obtained from FTIR is called an IR spectrum ranging from 4000 to 400 cm^{-1}.

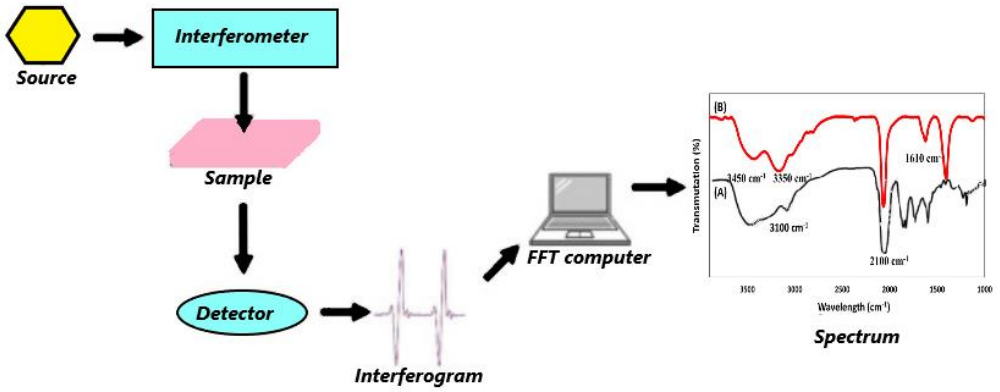

Figure 2.11 Schematic of FTIR spectroscope.

2.10.1 Principle of FTIR

The FTIR spectroscopy works on the principle of absorption of energy from infrared radiations that are in accordance with the sample, this leads to the vibrations (i.e., stretching, bending or sometimes both) of the covalent bonds between the molecules of the sample. The rest of the radiations that are not absorbed by the sample and were transmitted resultantly then gives us the FTIR spectra.

2.10.2 Mechanism of FTIR

The FTIR Spectrometer consists of IR source, an interferometer and a detector. The IR source provides the Infrared Radiation ranging from wavelength ~700nm to 1000nm.The Interferometer consists of the three mirrors i.e., a moving mirror, a stationary mirror and a beam splitter. When IR radiation beam is made incident on the beam splitter it is spitted into two beams of equal intensities. These two beams consist of a transmitted beam that is subjected to the stationary mirror whereas another beam is reflected to a moving mirror. The beams are then reflected back to the beam splitter after a complete cycle. These two beams

then interfere, both constructively and destructively, leading to a resultant IR radiation of a wide variety of intensities.

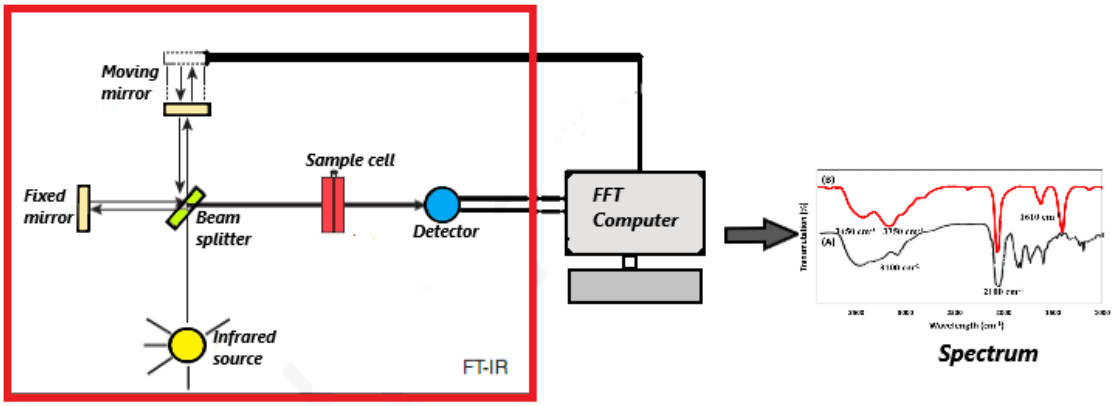

Figure 2.12 Interferometer of FTIR.

This process includes both constructive and destructive interference in accordance to the path difference between the two reflected beams[27]. The resultant IR radiation is made incident on the sample. The IR radiation has a wide range of energies, the sample absorbs only those energies that are similar to that of the molecule. This absorbed energy leads to vibrations in the covalent bonds between the samples. The rest of the IR radiation is then transmitted to the detector. The detector gives us the information about the absorbed energies by plotting a graph between Energy vs Time. This graph can be converted to Transmittance/Absorbance vs. Wavenumber by the application of mathematical transformation called Fourier Transform.

2.11 UV-Vis Spectroscopy

Ultraviolet-visible spectroscopy or ultraviolet-visible spectrophotometry (UV-Vis) refers to absorption spectroscopy or reflectance spectroscopy in the ultraviolet-visible spectral region. Ultraviolet-Visible (UV-VIS) Spectroscopy is an analytical method that can measure the analyte quantity depending on the amount of light received by the analyte.

Ultraviolet-visible spectroscopy or ultraviolet-visible spectrophotometry (UV-Vis) in the ultraviolet-visible spectral field refers to absorption spectroscopy or reflectance spectroscopy.

In the visible and neighboring (near-UV and near-infrared (NIR)) ranges, this means that it uses light.

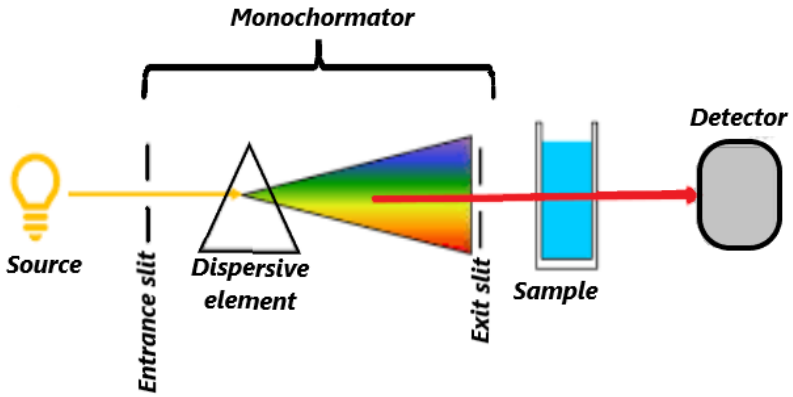

Figure 2.13 Schematic of UV-Vi's spectrometer.

2.11.1 Principle of UV Vis Spectroscopy

Basically, spectroscopy is related to the interaction of light with matter. As light is absorbed by matter, the result is an increase in the energy content of the atoms or molecules. When ultraviolet radiations are absorbed, this results in the excitation of the electrons from the ground state towards a higher energy state. Molecules containing π-electrons or nonbonding electrons (n-electrons) can absorb energy in the form of ultraviolet light to excite these electrons to higher anti-bonding molecular orbitals. The more easily excited the electrons, the longer the wavelength of light they can absorb.

There are three types of electronic transition which can be considered;

- Transitions involving p, s, and n electrons.
- Transitions involving charge-transfer electrons.
- Transitions involving d and f electrons

Beer-Lambert Law

The statement of the Beer-Lambert law can be written as follows: When a beam of monochromatic light is made incident on a solution that contains a substance that absorbs the

monochromatic light, the rate at which the intensity of the beam decreases along the thickness of the solution is directly proportional to the concentration of the absorbing substance in the solution and is also directly proportional to the intensity of the incident monochromatic radiation[28].

$$A = \varepsilon Lc$$

A is the amount of light absorbed for a particular wavelength by the sample

ε is the molar extinction coefficient

L is the distance covered by the light through the solution

c is the concentration of the absorbing species

As per the Beer-Lambert law, the greater the number of absorbing molecules (that have the ability to absorb light of a specific wavelength), the greater the extent of absorption of the radiation.

Chapter3

Methods for sample preparation

3.1 Introduction

This chapter provides an overview about the enhancement of photocatalytic activity of tungsten disulfide. The chapter also touches on the synthesis of Tungsten disulfide and the synthesis of its hybrids TiO_2/WS_2 and MoS_2/WS_2.The experimentation and characterization techniques verify the complete synthesis of the sample and other techniques acknowledge the photocatalytic activity regarding the samples.

3.2 Experimentaldetails

3.2.1 Synthesis of Tungsten Disulfide

Tungsten disulfide nanoflakes were synthesized viahydrothermal method. In which First, sodium tungstate (Na_2WO_4 $2H_2O$) (0.005 mol), hydroxylamine hydrochloride (NH_2OH. HCl) (0.01 mol), sulfourea (CH_4N_2S) (0.02 mol) were dissolved in 30 ml deionised water.

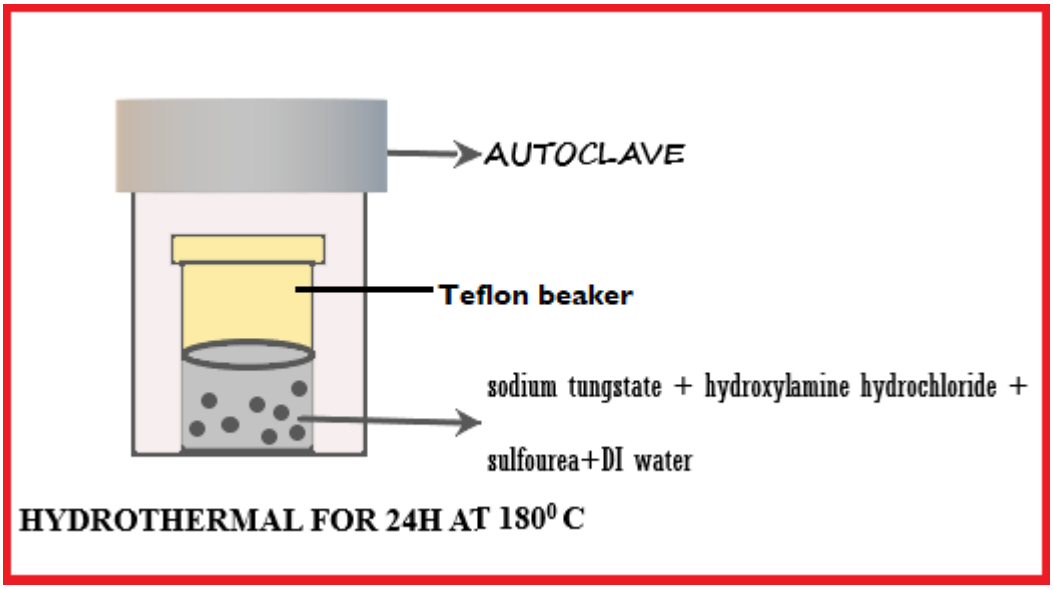

Figure 3.1Shows the schematic of synthesis of WS_2

The surfactant was then added into the solution under constant stirring. The pH value of the mixture was adjusted to approximately 6 by dropping 2 mol/L hydrochloric acid (HCl). The final solution was transferred into a 50 ml Teflon-lined stainless-steel autoclave, which was sealed and treated at 180^{O}C for 24 h[4], [6].

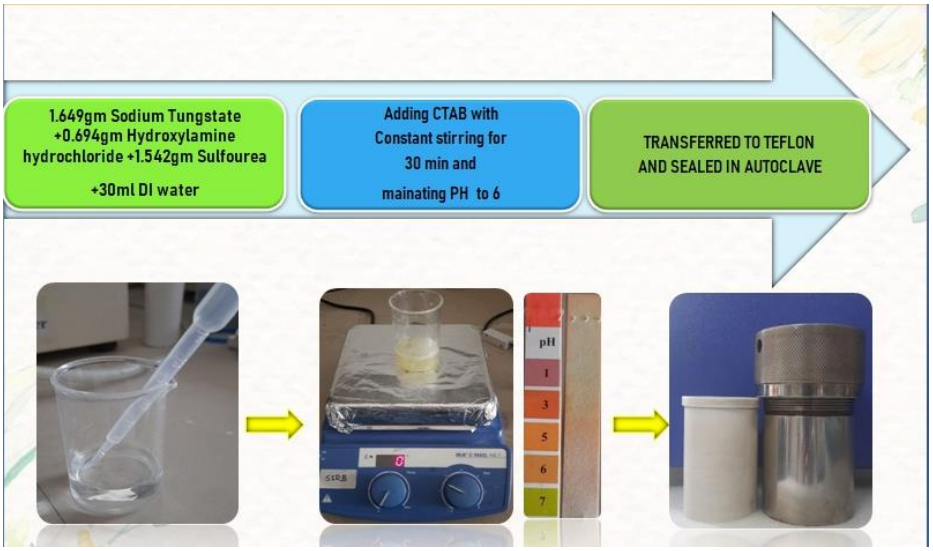

Figure 3.2 Reaction route for hydrothermal synthesis of WS_2.

The products obtained were grey in colour. After calcination, the as prepared samples were washed several times with distilled water and ethanol, and dried in air at60^{0}C for 10 h. The final product was further characterised using various characterization techniques.

Figure 3.3 Extraction process for WS_2

In our reaction the growth mechanism is an oxidation-reduction process that is responsible for the formation of WS_2 . The reaction route for the synthesis of WS_2 is as follow: -

$$Na_2WO_4 + 4CH_4N_2S + 4H_2O \rightarrow 4CO_2 + Na_2WS_4 + 8NH_3$$

$$Na_2WS_4 + 2NH_2OH.HCl \rightarrow WS_2 + N_2 + 2H_2O + 2H_2S + 2NaCl$$

The surfactant CTAB is added which usually plays the role as a template in the formation process of WS_2 conducting various morphologies. In general, the surfactant influences the interface energy and orientation of crystals. In our experiment when the amounts of CTAB substance added is 0.24g.

3.2.2 Synthesis of TiO_2/WS_2 Heterojunction:

The construction of heterojunction between TiO_2 and WS_2 also reveals remarkable enhancement in the photocatalytic activity. HereTiO_2 nanotubes were synthesised by electrochemical anodization (two electrode system) on Ti foils.

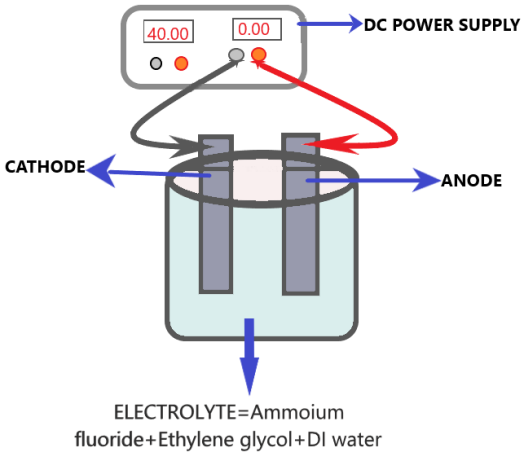

Figure 3.4 Annodization set up for TiO_2 nanotubes synthesis.

To obtain realiable and productive results the sample was ultrasonicated sequentially by acetone followed by IPA and lastly DI for 10-15 minutes each.The anodization of ti foils was carried out in an electrolytic bath with Ti foil as counter and working electrode.The electrolytic solution comprised of 0.1%wt of ammonium floride,95% ethylene glycoland 5% DI water. The anodization process was carried out at a consatant voltage of 40V for 2h resulting in formation of TiO_2 nanotubes on the substrate at the anode.

The sample was then rinsed with DI water and later for enhancement of crystallinity the preparedTiO_2nanotubes were anneled at 500^0Cfor 5 h in an air muffle furnance. Resulting in anatase crstalline phase of TiO_2 nanotubes.

Formation of heterojunction:

Further for the TiO_2andWS_2 heterostructure was achived via hydrothermal process.In order to carry out hydrothemal process, sodium tungstate ($Na_2WO_4.2H_2O$) (0.005 mol), hydroxylamine hydrochloride (NH_2OH. HCl) (0.01 mol), sulfourea (CH_4N_2S) (0.02 mol) were dissolved in 30 ml deionised water. The surfactant was then added into the solution under constant stirring. The pH value of the mixture was adjusted to approximately 6 by dropping 2 mol/L hydrochloric acid (HCl) and stirred for more tham 20 min,before poring the solution in the autoclave already placed with the anodised TiO_2nanotubes.

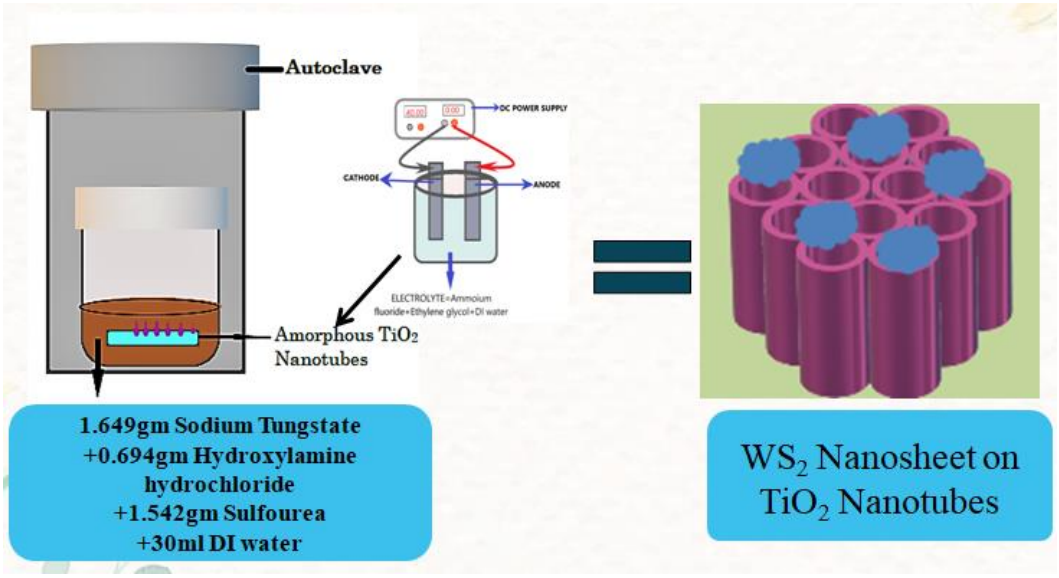

Figure 3.5 Synthesis route for TiO_2/WS_2hybid.

The hydrothermal process was carried out for 480min (8h) at 200^0 C in an oven followed by rinsing the prepared substrate with DI water.The substrate was later dried at 60^0 C for next 120 min.

3.2.3 Synthesis of MoS_2/WS_2Heterojunction

In a typical experiment, the MoS_2/WS_2 was prepared via hydrothermal synthesis in which, 0.08g Molybdenum disulfide, sodium tungstate (Na_2WO_4 $2H_2O$) (0.005 mol), hydroxylamine hydrochloride (NH_2OH. HCl) (0.01 mol), sulfourea (CH_4N_2S) (0.02 mol) were dissolved in 30 ml deionised water[8], [29]. The surfactant was then added into the solution under constant stirring. The pH value of the mixture was adjusted to approximately 6 by dropping 2 mol/L hydrochloric acid (HCl). The solution was stirred until it became clear and transparent by a magnetic stirrer. Later, the solution was poured in a teflon beaker 200 ml,which was then placed in an stainless steel autoclave. The autoclave was kept for 24h at 200C inside the oven. The autoclave was then allowed to cool down naturally. The obtained black/grey precipitate was then repeatedly and sequentially flushed with ethanol and DI respectively. At last, the obtained MoS_2/WS_2powderwas dried at 60 0 C for 12h.

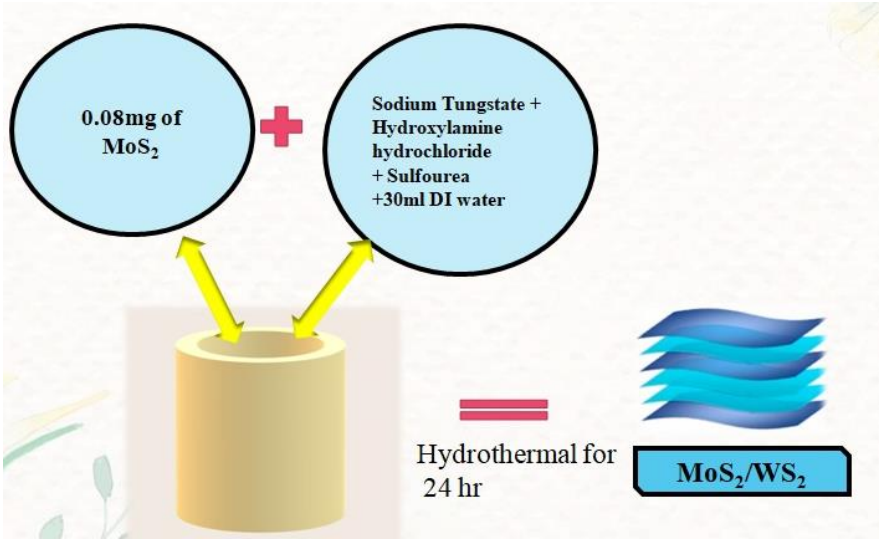

Figure 3.6 Synthesis route for MoS_2/WS_2hybrid.

3.3 Procedure for Photocatalysis

A comparative study was conducted to study the photodegradation behaviour of WS_2 against its hybrids MoS_2/WS_2 and TiO_2/WS_2. The photocatalytic activity of the samples was evaluated by monitoring the photodegradation of methylene blue (MB) in an aqueous solution. A photocatalyst (100 mg) was dispersed into the aqueous MB solution

(2.3×10^{-5} M, 20 mL) and then the mixed solution was illuminated while stirring. After a certain period of irradiation, an aliquot (5 mL) of the solution was sampled and measured for the absorbance of MB in each case.

Figure 3.7 (a) 0.02 g WS_2 as catalyst (b) TiO_2/WS_2 as photocatalyst (c) MoS_2/WS_2 as catalyst

3.3.1 WS_2 as catalysis

The photocatalytic performance of WS_2 was evaluated under visible light irradiation by assessing the degradation of MB. In a typical experiment, 0.02gm of WS_2catalyst was dispersed in MB aqueous solution through sonication treatment and the solution were stirred by continuous magnetic stirring for 30 min to ensure that an adsorption-desorption equilibrium between the dye solution and catalyst had been reached. Then, the above suspension was exposed under Xe lamp in the presence of catalyst. The solar light simulator equipped with a 300 W Xe lamp was used. The measured light intensity was 5 mW/cm^2at 10 cm from the source and after specified time intervals; 1mL aliquots were collected and the absorbance spectra were recorded and degradation efficiency was calculated using the equation C/C_0, where C is the absorbance of the solution after each interval time at λ_{max} and C_0 is the initial absorbance dye solution at λ_{max}.

3.3.2 TiO_2 /WS_2 as catalysis

The photocatalytic performance of TiO_2/WS_2 was evaluated with respect to the photodegradation of methylene blue at room temp under Xe light irradiation. In a typical experiment, 0.02gm of prepared TiO_2/ WS_2 catalyst was uniformly dispersed in MB aqueous solution through sonication treatment and the solution was stirred by continuous magnetic stirring for 1hr in darkness to ensure that an adsorption-desorption equilibrium between the dye solution and catalyst had been reached. Then, the above suspension was exposed under xenon lamp in the presence of catalyst, after specified time intervals; 1mL aliquotswere collected and the absorbance spectra were recorded and degradation efficiency was calculated using the equation C/C_0, where C is the absorbance of the solution after each interval time at λ_{max} and C_0 is the initial absorbance dye solution at $\lambda_{max.}$

3.3.3 MoS_2/WS_2 as catalysis

The photocatalytic performance of MoS_2/WS_2 was evaluated with respect to the photodegradation of methylene blue at room temp under Xe light irradiation. In a typical experiment, 0.02gm of prepared MoS_2/WS_2 catalyst was uniformly dispersed in MB aqueous solution through sonication treatment and the solution was stirred by continuousmagnetic stirring for 1hr in darkness to ensure that an adsorption-desorption equilibrium between the dye solution and catalyst had been reached. Then, the above suspension was exposed under xenon lamp in the presence of catalyst, after specified time intervals; 1mL aliquots were collected and the absorbance spectra were recorded and degradation efficiency was calculated using the equation C/C_0, where C is the absorbance of the solution after each interval time at λ_{max} and C_0 is the initial absorbance dye solution at λ_{max}.

Chapter 4

Results and Discussions

In this chapter, results of various characterizations done of prepared samples are shown and discussed briefly.

4.1 Scanning electron microscopy

The SEM was used to investigate the morphology of the asprepared WS_2. The SEM images of the as obtained samples are shown in Figure 4.1 at 4 different scanning ranges in the presence of surfactant. Sheet like morphology is quite evident from the images.The obtained thickness of nanosheets was found out to be ~4.8 nm.

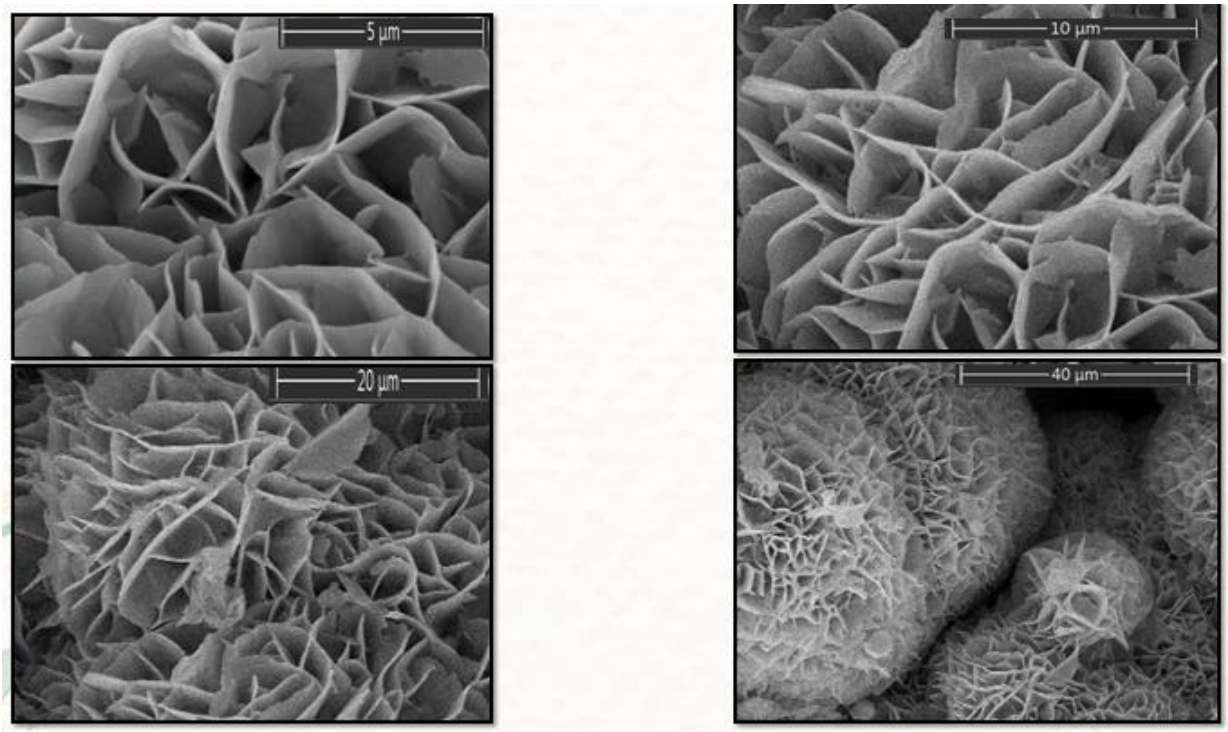

Figure 4.1 SEM images of prepared WS_2 nanosheets**.**

4.2 X-Ray Diffraction

The XRD data was collected using X-ray diffraction (XRD) (Bruker D8-Advance instrument with Cu K-α X-ay source). XRD patterns of all as-prepared WS_2 samples are shown in Fig 4.2. All of the diffraction peaks can be well indexed as those of the hexagonal phase of WS_2, consistent with the standard values JCPDS no. 08-0237.

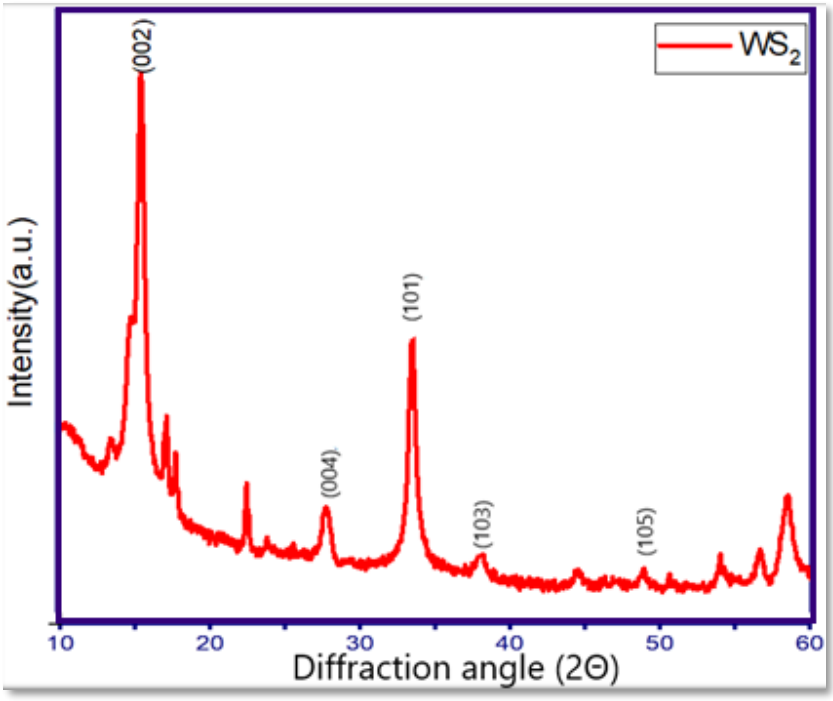

Figure 4.2 Obtained XRD OF WS_2

Diffraction Peaks at (002), (004), (101), (103) and (105) are the characteristic x-ray peaks for WS_2. (JCPDS no. 08-0237)

4.3 FTIR Spectroscopy

FTIR of samples was carried out for the prepared WS_2 and hybrids MoS_2/WS_2 and TiO_2/WS_2 and were recorded using an FTIR spectrometer.The obtained FTIR spectra for the three prepared samples is show in figure 4.3, in which the bands and peaks confirms the presence of WS_2 and the hybrids MoS_2/WS_2 and TiO_2/WS_2.

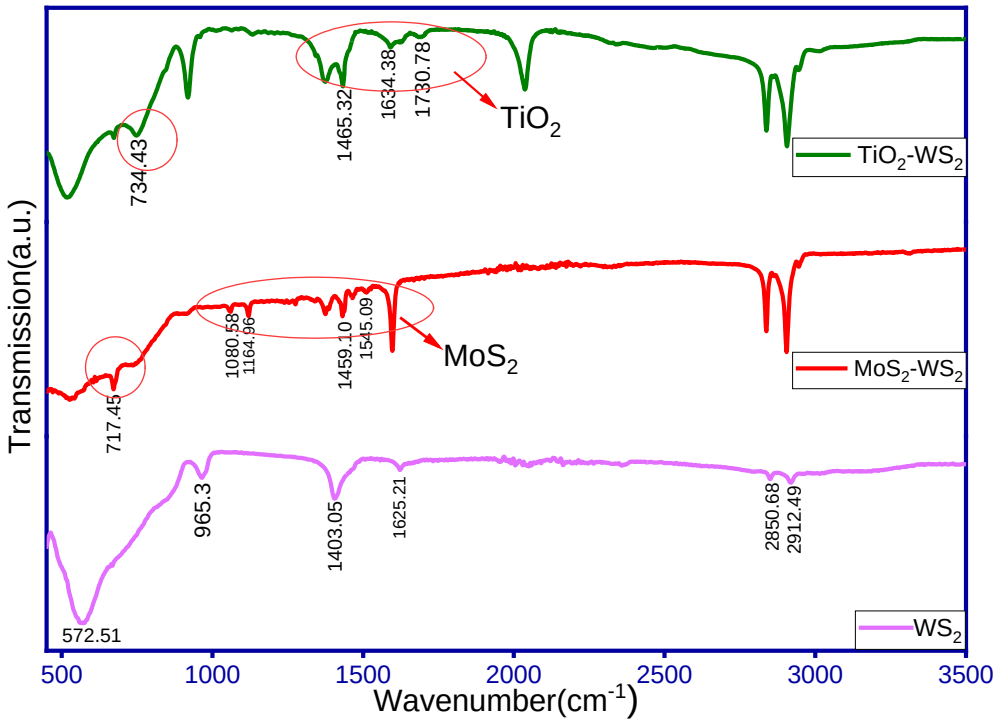

Figure 4.3 FTIR spectra of WS_2,MoS_2/WS_2 and TiO_2/WS_2

Figure 4.3 (a) shows the FTIR spectrum of WS2 .The band at 572cm^{-1} attributes to W-S bonds while the band at 965cm^{-1} corresponds to S-S bonds in WS_2 nanosheets.

Figure 4.3(b)shows the FTIR spectra for the hybrid MoS_2/WS_2. Circled band at 717.45cm^{-1},1080.5cm^{-1},1154cm^{-1},1459cm^{-1} and 1542.09cm^{-1} corresponds to MoS_2[26], [30]. The FTIR spectrum clearly shows the $MoS_2$and WS_2component in hybrid.

Figure 4.3 (c) shows the FTIR spectrum for the hybrid TiO_2/WS_2 and the circled band at 734.43cm^{1},1465.32cm^{-1},1634.38cm^{-1}, and1730.78cm^{-1}corresponds to TiO_2, and the FTIR spectrum for the hybrid shows the content to TiO_2 and WS_2 component in the hybrid.

4.4 UV-Vis Spectroscopy

UV-Vis spectroscopy of prepared samples was carried out to determine the Light Absorbance property which is shown in graph below (figure 4.4), which were in contrast to earlier literature work do.

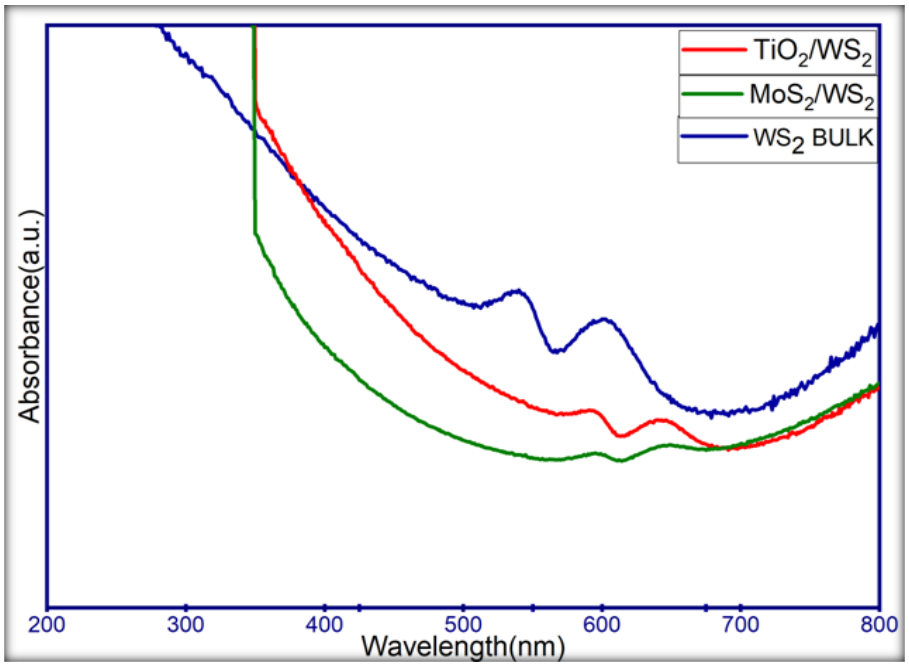

Figure 4.4 UV-Vis spectra of WS_2 ,MoS_2 /WS_2 and TiO_2 /WS_2.

The spectrum of WS_2 exhibits an intense optical absorption in the region between 500 to 700nm.with a characteristic peak located at 630 nm and the spectrum of hybrid MoS_2 /WS_2 and TiO_2 /WS_2 exhibits optical absorption in the region 550 to 650nm.

It is quite evident from UV-Vis plot that the absorption capacity of hybrid MoS_2/WS_2followed by TiO_2/WS_2 were comparatively more than that of WS_2.The band gaps, conduction band (CB), and valence band (VB) of WS_2, MoS_2/WS_2 and TiO_2/WS_2 which were estimated by Tauc's plots[22], [28]. The band gaps of the photocatalyst can be calculated using the following formula

$$(\alpha h\nu)1/n = A(h\nu - E_g)$$

Where α is the absorption coefficient, A is a constant, h is Planck's constant, Eg is the band energy, and ν is the frequency of the incident light. The value of n is decided by the property of the semiconductor. Anatase TiO2 is an indirect-band-gap semiconductor and its value of n is ½ while WS_2 and MoS_2 is a direct-band-gap semiconductor and its value of n is 2.

Calculated band gap (Approx.) using TAUC EQUATION:

Table4. 1 Calculated Band gap using Tauc's plot

Sample	Band gap(Calculated)
WS_2	1.3ev
MoS_2/WS_2	1.5ev
TiO_2/WS_2	2.6ev

Thus, it can be concluded that the addition of MoS_2 to WS_2, reach to decrease in the band gap which alternatively enhances its photocatalytic property as compared to TiO_2/WS_2 and WS_2.

4.5 IV curve for WS_2 and hybrids MoS_2/WS_2 and TiO_2/WS_2

The I-V curve is a graphical representation of the relationship between the voltage applied across an electrical device and the current flowing through it. It is one of the most common methods of determining how an electrical device functions in a circuit.

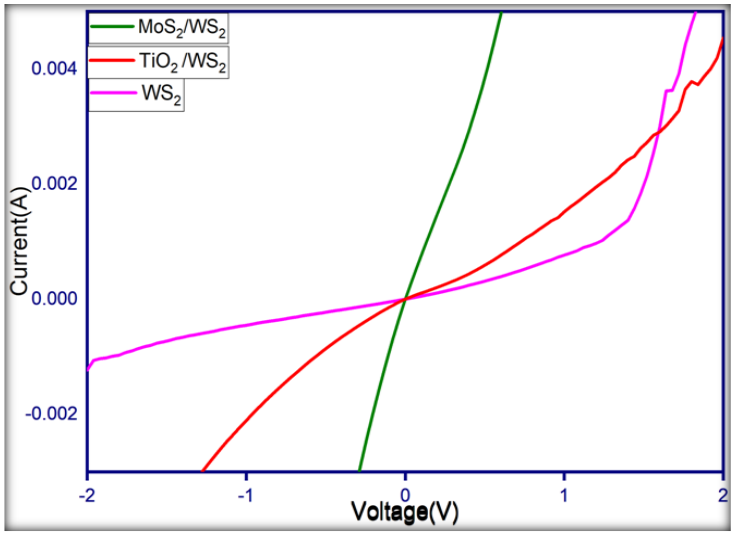

Figure 4.5 I-V curves for WS_2, TiO_2/WS_2 and MoS_2/WS_2.

A bias voltage was applied, with the Al layer serving as the upper electrode and the FTO layer serving as the lower electrode, which was grounded. Because the change in the current is approximately proportional to the applied voltage, a good conductive filament probably

existsand from the curves it can be concluded that the addition of MoS_2 followed by TiO_2 lead to increases in conductivity of WS_2which further enhanced the photocatalytic property.

4.6 Photocatalytic studies of WS_2 and hybrid TiO_2/WS_2 and MoS_2/WS_2

A comparative study was conducted to study the photodegradation behaviour of WS_2, TiO_2/WS_2 and MoS_2/WS_2. To evaluate the photocatalytic activity (figure 4.6), photocatalytic degradation of MB was carried out under visible-light irradiation. As shown the self-degradation of MB is negligible without photocatalyst. The WS_2 nanosheets show low adsorption capacity and comparatively low photocatalytic activity (Figure 4.6 a). In contrast, despite the unsatisfactory photocatalytic activity of WS_2, its adsorption capacity is higher than that of TiO_2 and MoS_2. The excellent absorption capacity of WS_2 was due to the MoS_2/WS_2 - followed by TiO_2/WS_2 heterojunction[5], [8],[19]. In addition, the photocatalytic performance of MoS_2/WS_2 and TiO_2/WS_2heterojunctions was obviously enhanced, especially $MoS_2/WS2$-0.10 (figure 4.6 b), which showed the highest photocatalytic activity as almost 100% MB was decomposed after 180 min irradiation under visible light followed by TiO_2/WS_2-0.10 (figure 4.6 c) in which MB decomposed more than 50% in 180 min irradiation under visible light .

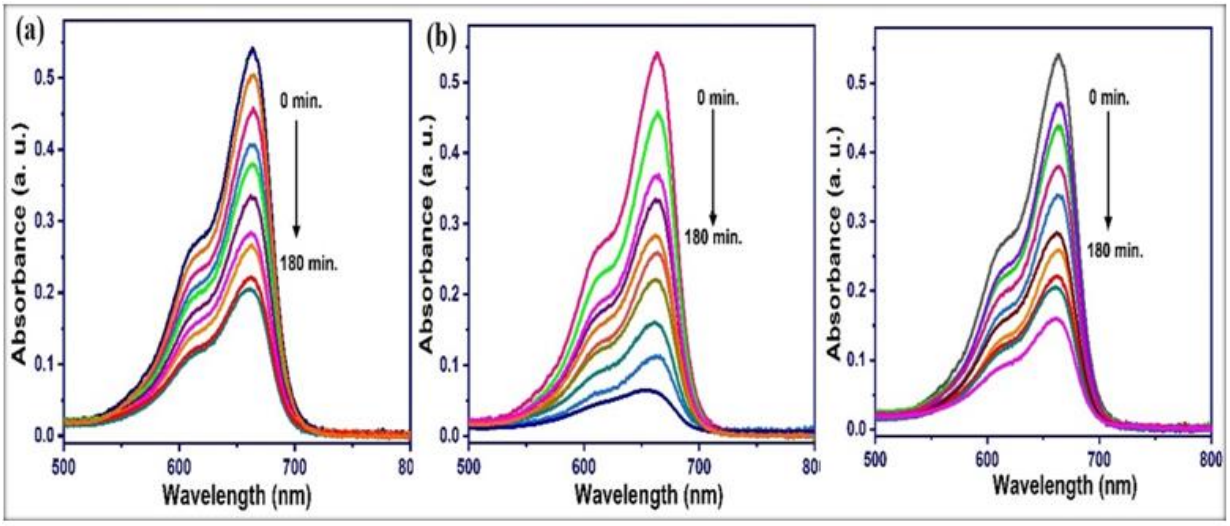

(a) WS_2 (b) MoS_2/WS_2 (c) TiO_2/WS_2

Figure 4.6Time-dependent UV–Vis spectra of MB dye.

The kinetic of the photo catalytic degradation of the MB was also analyzed using Langmuir–Hinshelwood expression Eq. (1),[35],[42]

$$(C_0/Ct) = kappt \quad (1)$$

where Co and Ct are the concentrations of MB dye at time t = 0 and t, respectively. The apparent rate constant (kapp) for the degradation of MB, was determined from the slope of the graph between ln(C_0/Ct) versus time.

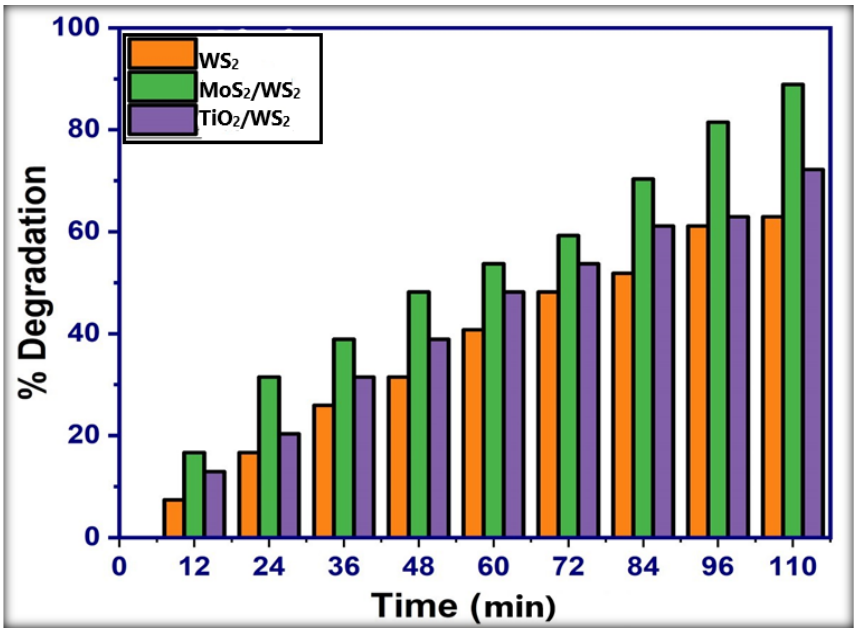

Figure 4.7 degradation efficiency (η) % vs. time plots of WS_2, MoS_2/WS_2 and TiO_2/WS_2

Thus, from photocatalytic studies, it is concluded that, the enhanced photocatalytic activity of WS_2 hybrids is making their place for photodegradation.

Chapter 5

Conclusions and Future Scope

5.1 Conclusions

In conclusion the hydrothermal method was used to synthesized WS_2 and hybrids $TiO_2/WS_2$and MoS_2/WS_2. XRD was carried out to find the chemical composition and phase of WS_2which was evidently obtained and consistent with the standard values JCPDS no. 08-0237[6]. The SEM results shows us the sheet like morphology of obtained WS_2.The FTIR results evidently referred that we were able to synthesize WS_2, TiO_2/WS_2 and MoS_2/WS_2 in the FNR lab via hydrothermal method.The IV characteristic of the synthesis samples showed that the conductivity of MoS_2/WS_2 was most followed by TiO_2/WS_2 hybrid and WS_2 respectively. The increase in conductivity led to formation of more electron-hole pair formation in MoS_2/WS_2 to that of TiO_2/WS_2 and WS_2.

Also, the surface to volume area of WS_2 increased due to the addition of another 2D material MOS_2 which provided most surface area as catalysts for degradation. Also, TiO_2/WS_2 hybrid also increased the surface to volume area more that WS_2 but not as that of MoS_2/WS_2.

The IV data results were strengthened by UV-Vis spectra of MoS_2/WS_2, TiO_2/WS_2 and WS_2 as photocatalyst for degrading MB dye in a time course of 180 min.

From the photocatalytic studies it was found that MB dye was degraded almost 100% with MoS_2/WS_2 as photocatalyst whereas that 50% and less than 50% for TiO_2/WS_2 and WS_2 respectively as photocatalyst for the same time course.

Hence it the best photodegradation of MB was obtained in the presence MoS_2/WS_2 as catalyst which may be due the most surface to volume area of MoS_2/WS_2 and due to the highest conductivity among all three catalysts.

5.1 Future scope

The growth of 2-dimensional hybrids and heterostructures are needed to be studiedin detail. By optimizing the growth parameters and by making heterostructure of $WS_2$with other material. The photocatalytic properties of WS_2 hybrids and heterostructures are needed to beoptimized for energy harvesting device applications CO_2 reduction, hydrogen reduction etc.The electrochemical studied of hybrids is needed to be studied in detail. The catalytic properties of WS_2based hybrids are needed to be optimized for phototype devices and energy harvesting devices. The growth of periodically segmented WS_2 by Arduino are need to studied for energyharvesting devices.

References

[1] S. J. McDonnell and R. M. Wallace, “Atomically-thin layered films for device applications based upon 2D TMDC materials,” Thin Solid Films, vol. 616, pp. 482–501, 2016, doi: 10.1016/j.tsf.2016.08.068.

[2] S. Two-dimensional, D. Jariwala, V. K. Sangwan, L. J. Lauhon, T. J. Marks, and M. C. Hersam, “Emerging Device Applications for semiconducting 2D TMDCs,” ACS Nano, vol. 8, no. 2, pp. 1102–1120, 2014, [Online]. Available: http://www.ncbi.nlm.nih.gov/pubmed/24476095

[3] X. Li, X. Li, Z. Li, J. Wang, and J. Zhang, “WS2 nanoflakes based selective ammonia sensors at room temperature,” Sensors Actuators, B Chem., vol. 240, pp. 273–277, 2017, doi: 10.1016/j.snb.2016.08.163.

[4] M. O’Brien et al., “Plasma assisted synthesis of WS2 for gas sensing applications,” Chem. Phys. Lett., vol. 615, pp. 6–10, 2014, doi: 10.1016/j.cplett.2014.09.051.

[5] T. Järvinen, G. S. Lorite, J. Peräntie, and G. Toth, “WS 2 and MoS 2 thin fi lm gas sensors with high response to NH 3 in air at low temperature,” 2016.

[6] S. Cao, T. Liu, S. Hussain, W. Zeng, X. Peng, and F. Pan, “Hydrothermal synthesis of variety low dimensional WS2 nanostructures,” Mater. Lett., vol. 129, pp. 205–208, 2014, doi: 10.1016/j.matlet.2014.05.013.

[7] J. H. Kim, A. Mirzaei, H. W. Kim, and S. S. Kim, “Realization of Au-decorated WS2 nanosheets as low power-consumption and selective gas sensors,” Sensors Actuators, B Chem., vol. 296, p. 126659, 2019, doi: 10.1016/j.snb.2019.126659.

[8] N. Chaudhary and M. Khanuja, “ Architectural Design of Photodetector Based on 2D (MoS 2 Nanosheets)/1D (WS 2 Nanorods) Heterostructure Synthesized by Facile Hydrothermal Method ,” J. Electrochem. Soc., vol. 166, no. 14, pp. B1276–B1285, 2019, doi: 10.1149/2.0341914jes.

[9] D. L. Kolesnik et al., “The effect of 2D tungsten disulfide nanoparticles on Lewis lung carcinoma cells: In vitro,” RSC Adv., vol. 11, no. 27, pp. 16142–16150, 2021, doi: 10.1039/d1ra01469b.

[10] K. J. Huang, L. Wang, J. Li, and Y. M. Liu, “Electrochemical sensing based on layered

MoS2-graphene composites," Sensors Actuators, B Chem., vol. 178, pp. 671–677, 2013, doi: 10.1016/j.snb.2013.01.028.

[11] Q. Gong et al., "Ultrathin MoS2(1-x)Se2x Alloy Nanoflakes for Electrocatalytic Hydrogen Evolution Reaction," ACS Catal., vol. 5, no. 4, pp. 2213–2219, 2015, doi: 10.1021/cs501970w.

[12] E. Pollmann, L. Madauß, V. Zeuner, and M. Schleberger, Strain in single-layer MoS2 flakes grown by chemical vapor deposition. Elsevier, 2018. doi: 10.1016/B978-0-12-409547-2.14175-7.

[13] X. Li and H. Zhu, "Two-dimensional MoS2: Properties, preparation, and applications," J. Mater., vol. 1, no. 1, pp. 33–44, 2015, doi: 10.1016/j.jmat.2015.03.003.

[14] M. Faraz, H. H. Singh, and N. Khare, "A progressive strategy for harvesting mechanical energy using flexible PVDF-rGO-MoS2 nanocomposites film-based piezoelectric nanogenerator," J. Alloys Compd., vol. 890, p. 161840, 2022, doi: 10.1016/j.jallcom.2021.161840.

[15] A. Rai, H. C. P. Movva, A. Roy, D. Taneja, S. Chowdhury, and S. K. Banerjee, Progress in contact, doping and mobility engineering of MoS2: An atomically thin 2D semiconductor, vol. 8, no. 8. 2018. doi: 10.3390/cryst8080316.

[16] J. Zhu et al., "Preparation of PVDF/TiO2 nanofibers with enhanced piezoelectric properties for geophone applications," Smart Mater. Struct., vol. 28, no. 8, 2019, doi: 10.1088/1361-665X/ab29a9.

[17] B. Feng, C. Liu, W. Yan, J. Geng, and G. Wang, "MoS2 nanotubes loaded with TiO2 nanoparticles for enhanced electrocatalytic hydrogen evolution," RSC Adv., vol. 9, no. 45, pp. 26487–26494, 2019, doi: 10.1039/c9ra05041h.

[18] P. Bamola et al., "Mixed-Phase TiO2Nanotube-Nanorod Hybrid Arrays for Memory-Based Resistive Switching Devices," ACS Appl. Nano Mater., vol. 3, no. 11, pp. 10591–10604, 2020, doi: 10.1021/acsanm.0c01648.

[19] M. Shanmugam, T. Bansal, C. A. Durcan, and B. Yu, "MoS2 / TiO2 nanoparticle composite bulk heterojunction solar cell," Proc. IEEE Conf. Nanotechnol., 2012, doi: 10.1109/NANO.2012.6322088.

[20] L. Yang, H. Ji, K. Zhu, J. Wang, and J. Qiu, "Dramatically improved piezoelectric

properties of poly(vinylidene fluoride) composites by incorporating aligned TiO2@MWCNTs," Compos. Sci. Technol., vol. 123, pp. 259–267, 2016, doi: 10.1016/j.compscitech.2015.11.032.

[21] O. Zakir et al., "Fabrication of TiO2Nanotube by Electrochemical Anodization: Toward Photocatalytic Application," J. Nanomater., vol. 2020, 2020, doi: 10.1155/2020/4745726.

[22] Z. Liu et al., "Amorphous MoSx-Coated TiO2 Nanotube Arrays for Enhanced Electrocatalytic Hydrogen Evolution Reaction," J. Phys. Chem. C, vol. 122, no. 24, pp. 12589–12597, 2018, doi: 10.1021/acs.jpcc.8b01678.

[23] Y. Tian, Y. Song, M. Dou, J. Ji, and F. Wang, "Enhanced photo-assistant electrocatalysis of anodization TiO 2 nanotubes via surrounded surface decoration with MoS 2 for hydrogen evolution reaction," Appl. Surf. Sci., vol. 433, pp. 197–205, 2018, doi: 10.1016/j.apsusc.2017.09.259.

[24] Y. Shang, J. Xia, Z. Xu, and W. Chen, "Hydrothermal synthesis and characterization of quasi-1-D tungsten disulfide nanocrystal," J. Dispers. Sci. Technol., vol. 26, no. 5, pp. 635–639, 2005, doi: 10.1081/DIS-200057684.

[25] N. T. Shelke and B. R. Karche, "Hydrothermal synthesis of WS2/RGO sheet and their application in UV photodetector," J. Alloys Compd., vol. 653, pp. 298–303, 2015, doi: 10.1016/j.jallcom.2015.08.255.

[26] T. Xu et al., "The ultra-high NO2 response of ultra-thin WS2 nanosheets synthesized by hydrothermal and calcination processes," Sensors Actuators, B Chem., vol. 259, no. 2, pp. 789–796, 2018, doi: 10.1016/j.snb.2017.12.070.

[27] S. Mourdikoudis, R. M. Pallares, and N. T. K. Thanh, "Characterization techniques for nanoparticles: Comparison and complementarity upon studying nanoparticle properties," Nanoscale, vol. 10, no. 27, pp. 12871–12934, 2018, doi: 10.1039/c8nr02278j.

[28] L. Soltane and F. Sediri, "Rod-like nanocrystalline B-VO2: Hydrothermal synthesis, characterization and electrochemical properties," Mater. Res. Bull., vol. 53, pp. 79–83, 2014, doi: 10.1016/j.materresbull.2014.01.046.

[29] Y. Zhao et al., "Convenient Synthesis of WS2-MoS2 Heterostructures with Enhanced

Photocatalytic Performance," J. Phys. Chem. C, 2019, doi: 10.1021/acs.jpcc.9b08101.

[30] N. Lu, H. Guo, L. Wang, X. Wu, and X. C. Zeng, "Van der Waals trilayers and superlattices: Modification of electronic structures of MoS2 by intercalation," Nanoscale, vol. 6, no. 9, pp. 4566–4571, 2014, doi: 10.1039/c4nr00783b.

[31] T.Theivasanthi, M.Alagar Titanium dioxide (TiO2) Nanoparticles XRD Analyses: An Insight https://doi.org/10.48550/arXiv.1307.1091

[32] BehzadPourabbas BabakJamshidi Preparation of MoS2 nanoparticles by a modified hydrothermal method and the photo-catalytic activity of MoS2/TiO2 hybrids in photo-oxidation of phenol https://doi.org/10.1016/j.cej.2007.05.028

[33] H. J. Leamy Charge collection scanning electron microscopy https://doi.org/10.1063/1.331667

[34] Catherine Berthomieu & Rainer Hienerwadel Fourier transform infrared (FTIR) spectroscopy https://doi.org/10.1007/s11120-009-9439-x

[35] L. Andrew Lyon, Christine D. Keating, Audrey P. Fox, Bonnie E. Baker, Lin He, Sheila R. Nicew arner, Shaw n P. Mulvaney, and Michael J. Natan* Raman Spectroscopy https://doi.org/10.1021/a10000155

[36] Shouhua Feng and Ruren Xu New Materials in Hydrothermal Synthesishttps://doi.org/10.1021/ar0000105

[37] Ngoc Tai Ly1, Van Chien Nguyen1, Thi Hoa Dao1, Le Hong Hoang To1, Duy Long Pham1, Hung Manh Do1, Dinh Lam Vu1 and Van Hong Le1 Optical properties of TiO2 nanotube arrays fabricated by the electrochemical anodization method

https://doi.org/10.1088/2043-6262/5/1/015004

[38]Azrina Abd Aziz Synthesis and Characterization of TiO2 Nanotube Using Electrochemical Anodization Method https://doi.org/10.15282/ijets.v5i3.1136

[39] WonbongChoi NitinChoudhary GangHeeHan JuhongPark1DejiAkinwande Young HeeLee Recent development of two-dimensional transition metal dichalcogenides and their applications https://doi.org/10.1016/j.mattod.2016.10.002

[40] Deep Jariwala Vinod K. Sangwan Lincoln J. Lauhon Tobin J. Marks and Mark C. Hersam Emerging Device Applications for Semiconducting Two-Dimensional

Transition Metal Dichalcogenides https://doi.org/10.1021/nn500064s

[41] Ashraf A.IsmailFrederick R.van de VoortJacquelineSedman Fourier transform infrared spectroscopy: Principles and applicationshttps://doi.org/10.1016/S0167-9244(97)80013-3

[42] Ruchita S.DasY.K.Agrawal Raman spectroscopy: Recent advancements, techniques and applications https://doi.org/10.1016/j.vibspec.2011.08.003

[43] X. Zhang, W. P. Han, J. B. Wu, S. Milana, Y. Lu, Q. Q. Li, A. C. Ferrari, and P. H. Tan Raman spectroscopy of shear and layer breathing modes in multilayer MoS2https://doi.org/10.1103/PhysRevB.87.115413

[44] Xiaobo Chen and Samuel S. Mao Titanium Dioxide Nanomaterials: Synthesis, Properties, Modifications, and Applications https://doi.org/10.1021/nn500064s

[45] Chenhao Jin, Eric Yue Ma, Ouri Karni, Emma C. Regan, Feng Wang Ultrafast dynamics in van der Waals heterostructures https://doi.org/10.1038/s41565-018-0298-5

[46] Abd Aziz Synthesis and Characterization of TiO2 Nanotube Using Electrochemical Anodization Method https://doi.org/10.15282/ijets.v5i3.1136